Quasinormal modes of rotating accelerating black holes

Wei Xiong[*] and Peng-Cheng Li[†]

School of Physics and Optoelectronics, South China University of Technology,
Guangzhou 510641, People's Republic of China

This paper studies the quasinormal mode spectrum of the scalar perturbation on the background of the rotating accelerating black holes. The quasinormal frequency ω and the separation constant λ are calculated using two methods: the continued fractions method and the direct integration method. The spectrum is found to include three families of modes: the photon sphere modes, the acceleration modes, and the near extreme modes. We investigate the effects of back hole parameters such as spin and acceleration. Empirical formulas are presented for the numerical results, specifically for the acceleration modes in the small black hole limit or the near extreme modes in the extreme black hole limit. An interesting phenomenon known as eigenvalue repulsion is observed when the acceleration modes intersect with the near extreme modes at certain parameter values. The strong cosmic censorship conjecture for spinning C-metric is respected.

I. INTRODUCTION

Black holes (BHs) are compact objects characterized by an event horizon in the Universe. Recently, BHs have gained increasing attention in academia, owing to the detection of gravitational waves [1–3], as well as the first depiction of the BH picture [4]. According to the uniqueness theorem [5], in four-dimensional spacetime, the most general stationary asymptotically flat BH solution to the electrovacuum Einstein field equations is the Kerr-Newman BH [6]. The solution is uniquely characterized by the mass, angular momentum, and the charge. However, the most general solution including more parameters is the Plebański-Demiański metric in the frame of general relativity [7,8]. This family of metric is of Petrov type D with an aligned electromagnetic field and cosmological constant Λ [8–10]. One can reduce the Plebański-Demiański metric to different solutions with relevant physical interpretations by certain transformations and limiting procedures.

An intriguing solution called the spinning C-metric belongs to the general Plebański-Demiański family [11–14]. It describes a boost-rotation-symmetric stationary spacetime that contains two causally separated rotating BHs accelerating away from each other in opposite spatial directions [15]. This metric is useful for understanding the behavior of moving and accelerating BHs, such as those resulting from a BH superkick [16–19]. A superkick may arise from the dynamical processes such as scattering, grazing collision, or merger of two equal-mass BHs [20]. During these events, anisotropic gravitational radiation is emitted, leading to a net

emission of linear momentum. As a result, the final remnants undergo gradual acceleration and acquire a recoil velocity.

At the late time stage of such dynamical procedure, the remnant BHs can be described by a perturbed state (e.g., the ringdown stage of the binary BH merger). Besides, BHs are always perturbed by macroscopic objects or fields in the astronomical environment. The perturbations on the background of BHs generate the radiation wave characterized by a set of damped oscillation frequencies, known as quasinormal modes (QNMs) [21–24]. According to the no-hair theorem [25], QNMs are only related to the parameters of the background BH, but not to the specific configuration of perturbations. QNMs provide a unique perspective of BH observations and help us to determine the parameters of observed BHs [26,27].

The QNM spectrum of BHs with acceleration and charge, namely the charged C-metric, has been examined in [28,29]. The charge C-metric possesses an acceleration horizon that is analogous to the cosmological horizon of Reissner-Nordström–de Sitter (RN-dS) BH. This similarity enables the QNM spectrum to include three distinct families of QNMs (the photon sphere modes, the acceleration modes, and the near extreme modes) [30,31]. The acceleration horizon acts as a boundary that separates the causality between the exterior and interior regions. Imposing the outgoing boundary condition at the acceleration horizon leads to an exponential-law late time behavior of perturbation for the charged C-metric, instead of a power-law tail under the time domain analysis [28].

However, realistic BHs in our Universe are typically nearly neutral and rotating, with electromagnetic charge quickly neutralized by various mechanisms such as

---
[*]202210187053@mail.scut.edu.cn
[†]Corresponding author: pchli2021@scut.edu.cn

environment plasma, Schwinger pair creation, or Hawking evaporation [31]. The spin of BH originates from the collapse of rotating objects [32–34], the final angular momentum of binary compact object mergers [35,36], or even accretion of matter onto the BH.

In this paper, we study the scalar perturbations that are governed by a separable master equation on the background of rotating accelerating BHs. The corresponding QNM spectrum is numerically investigated in full parameter space instead analytically approximated in the Nariai-type near extreme limit [37]. The QNM frequency and the separation constant, which depend on each other, are determined by two methods: the continued fractions method and the direct integration method.

The QNM spectrum includes three distinct families of modes: the photon sphere modes, the acceleration modes, and the near extreme modes. The acceleration modes were previously found in the boosted spacetime [28,29]. When the BH spin becomes large, the photon sphere modes and the near extreme modes branch off from the same set of QNMs [38,39]. The photon sphere modes are associated with the peaks of the potential barrier, while the near extreme modes are related to the near horizon geometry of the Kerr BH.

We find an intriguing phenomenon called eigenvalue repulsion, which emerges from the intersection between the acceleration modes and the near extreme modes. The eigenvalue repulsion is a well-established phenomenon in the energy level problems of simple quantum mechanical models with self-adjoint Hamiltonians. This phenomenon within the QNM spectrum governed by non-self-adjoint operators, was first reported by Dias *et al.* in the cases of Kerr-Newman BHs recently [40,41] and (higher-dimensional) Kerr-dS BHs [42]. For the rotating accelerating BHs, the eigenvalue repulsion arises as a result of the intersection between acceleration modes and near extreme modes in the complex plane.

The QNMs can also be used to examine the strong cosmic censorship (SCC) conjecture, which is associated with an infinite blueshift of perturbations at the Cauchy horizon [43,44]. Recent works demonstrate that the SCC is violated by nearly extreme RN-dS BHs when considering neutral scalar perturbations [30]. The exponential decay of these perturbations can suppress the blueshift amplifications at the Cauchy horizon. However, the violation of SCC is saved by the presence of charged massive scalars [31] and SCC is respected by perturbations on the background of Kerr-dS BHs [45]. In accelerating spacetimes, there also exists a competitive mechanism between the blueshift instability and the exponential decay of scalar perturbations at the Cauchy horizon [28]. The SCC conjecture is violated when considering scalar perturbations on the charged C-metric [46] or conformally scalar accelerating BHs with neither charge nor rotation [47]. In this paper, we investigate the spinning C-metric for perturbations.

The remainder of this paper is organized as follows. We review the spinning C-metric and the perturbation equations separated from the master equation in Sec. II. In Sec. III, the two methods we used are introduced. The results are presented in Sec. IV. We give a summary and some discussions in Sec. V. By convention, we employ the geometric units $G = c = 1$.

II. ACCELERATING BLACK HOLE

A. Spinning C-metric

The spinning C-metric can be obtained by imposing certain constraints on the Plebański-Demiański metric [8]. One can express the line element corresponding to the spinning C-metric by using the Boyer-Lindquist-type coordinates (t, r, θ, ϕ) [48],

$$
\begin{aligned}
ds^2 = \frac{1}{\Omega} \Bigg(& \frac{1}{\Sigma}(Q - a^2 P \sin^2\theta) dt^2 \\
& - \frac{2a\sin^2\theta}{\Sigma}(Q - P(r^2 + a^2)) dt d\phi \\
& - \frac{\sin^2\theta}{\Sigma}(P(r^2 + a^2)^2 - a^2 Q \sin^2\theta) d\phi^2 \\
& - \frac{\Sigma}{Q} dr^2 - \frac{\Sigma}{P} d\theta^2 \Bigg),
\end{aligned}
\tag{1}
$$

with the definitions of functions

$$
\begin{aligned}
& \Omega = 1 - \alpha r \cos\theta, \qquad \Sigma = r^2 + a^2 \cos^2\theta, \\
& P = 1 - 2\alpha M \cos\theta + a^2 \alpha^2 \cos^2\theta, \\
& Q = \Delta(1 - \alpha^2 r^2), \qquad \Delta = r^2 - 2Mr + a^2,
\end{aligned}
\tag{2}
$$

where the parameters M, α, and a are related to the BH mass, acceleration, and rotation, respectively. The spinning C-metric reduces to the nonrotating vacuum C-metric when $a = 0$, to the vacuum Kerr metric when $\alpha = 0$, and to the Schwarzschild metric when both a and α vanish.

There are conical singularities at the axis $\theta = 0$ and $\theta = \pi$, indicating the existence of deficit angles. Without loss of generality, we specify $\phi \in [0, 2\pi/P(\pi))$ to remove the conical singularity at $\theta = \pi$. However, at the opposite pole ($\theta = 0$), the deficit angle persists and it is not possible to remove both conical singularities simultaneously [28].

According to the expression of Q, we have $r_\pm = M \pm \sqrt{M^2 - a^2}$ as the outer event horizon and the inner Cauchy horizon and $r_\alpha = \alpha^{-1}$ as the acceleration horizon related three null hypersurfaces of the rotating accelerating BH. Our calculation is limited to the spherical corona $r_+ < r < r_\alpha$ [or $\alpha < \alpha_{\text{ext}} \equiv 1/(1 + \sqrt{M^2 - a^2})$] by convention. Such constraint gives $Q > 0, P(\theta) > 0$ for $r > 0, \theta \in [0, \pi]$.

The surface gravity at each horizon $r_i \in \{r_-, r_+, r_\alpha\}$ is given by

$$\kappa_i \equiv \left. \frac{|\partial_r Q(r)|}{2(r^2 + a^2)} \right|_{r=r_i}. \qquad (3)$$

B. Perturbation equation

A separable master equation, describing the massless field perturbations to the spinning C-metric with any spin s, has been established by Bini *et al.* [48] in terms of gauge- and tetrad-invariant quantities. This approach based on the Newman-Penrose formalism was originally developed to study perturbations on the background of the Kerr BH for any spin. Imposing the separable solutions

$$\varphi(t, r, \theta, \phi) = \Omega^{2s+1} e^{-i\omega t} e^{im\phi} R(r) \frac{Y(\theta)}{\sqrt{P}}, \qquad (4)$$

the master equation can be separated into the radial part

$$0 = Q^{-s} \frac{d}{dr}\left(Q^{s+1} \frac{dR(r)}{dr}\right) + V_{\text{rad}}(r)R(r), \qquad (5)$$

$$\begin{aligned}
V_{\text{rad}}(r) = &-2r\alpha^2(r-M)(1+s)(1+2s) \\
&+ \frac{((a^2+r^2)\omega - am)^2}{Q} \\
&- 2is\left(-\frac{am\partial_r Q}{2Q} + \frac{\omega M(r^2 - a^2)}{\Delta} - \frac{\omega r\sigma}{1 - \alpha^2 r^2}\right) \\
&+ 2\lambda,
\end{aligned} \qquad (6)$$

and the following angular part:

$$0 = \frac{1}{\sin\theta} \frac{d}{d\theta}\left(\sin\theta \frac{dY(\theta)}{d\theta}\right) + V_{\text{ang}}(\theta)Y(\theta), \qquad (7)$$

$$\begin{aligned}
V_{\text{ang}}(\theta) = &-\frac{2\lambda - s(1 - \alpha^2 a^2)}{P} \\
&+ \frac{1}{P^2}\left(\frac{-\sigma^2 s^2 \cos^2\theta + 2\sigma s w \cos\theta - w^2 \cos^2\theta}{\sin^2\theta}\right. \\
&+ z^2 \cos^2\theta - 2s\sigma z \cos\theta - (z + w - 4s\alpha M)^2 \\
&+ \left.\alpha^2((M^2 - a^2)\sin^2\theta + 4sa^2 \cos\theta(2s\alpha M - w))\right),
\end{aligned} \qquad (8)$$

where $z \equiv a\omega + s\alpha M$, $w \equiv 2s\alpha M - m$, and $\sigma \equiv 1 + a^2\alpha^2$. The spin-weight parameter s of the above equations is set to be 0 for the scalar perturbations in this study. The parameter ω signals the oscillation frequency. To remove the conical singularity along $\theta = \pi$, the azimuthal separation constant m needs to be of the form $m \equiv m_0 P(\pi)$, where m_0 is a positive integer.

The separation constant λ, as an eigenvalue of the spin-weighted spheroidal harmonics in the generalized Teukolsky formalism, depends on ω in the presence of a nonzero BH spin parameter a. λ can be written in familiar form for certain limit cases of the parameters, e.g., $\lambda = -l(l+1)/2$ with $a = 0$, $\alpha = 0$ for the Schwarzschild case [48], $\lambda = (-A_{lm} - a^2\omega^2 + 2am\omega)/2$ with $\alpha = 0$ for the Kerr case [49], and $\lambda = (1/3 - \lambda')/2$ with $a = 0$ for the nonspinning C-metric case [28,29]. The symbols (l, A_{lm}, λ') represent the separation constant for corresponding references.

The calculation of QNM frequency ω is the eigenvalue problems of (5) and (7) related to the QNM boundary condition. Physically, only purely ingoing waves can exist at the event horizon, while at the acceleration horizon, the purely outgoing wave uniquely presents

$$R(r) \sim \begin{cases} (r - r_+)^A, & r \to r_+, \\ (r_\alpha - r)^B, & r \to r_\alpha, \end{cases} \qquad (9)$$

with $A = -i[\omega - am/(r_+^2 + a^2)]/2\kappa_+$ and $B = -i[\omega - am/(r_\alpha^2 + a^2)]/2\kappa_\alpha$. We also require the solution to be regular at the interval boundaries of θ,

$$Y(\theta) \sim \begin{cases} \left(\frac{\cos\theta - 1}{2}\right)^C, & \theta \to 0, \\ \left(\frac{\cos\theta + 1}{2}\right)^D, & \theta \to \pi, \end{cases} \qquad (10)$$

where $C = \frac{m}{2 - 4M\alpha + 2a^2\alpha^2}$ and $D = \frac{m}{2 + 4M\alpha + 2a^2\alpha^2}$, to avoid the disastrous divergence of solutions at $\theta = 0, \pi$. The more evident boundary behavior discussion can be found in [48] (also in [28] for nonspinning C-metric) where the perturbation equation was transformed into the Schrödinger-like form.

Remarkably, the separation content λ and the QNM ω are eigenvalues entangled with each other for the two equations with proper boundary conditions (9) and (10). λ also depends on the acceleration α of the accelerating BHs. Our treatment follows the way of Leaver [49], i.e., given a tentative value of ω, we solve λ from (7) and then judge whether the corresponding solution of ω satisfies the QNM conditions (9). The judgment of the two methods is similar: the continued fractions equation (15) tends to be 0 for the continued fractions method and the resulting determinant (19) tends to be 0 for the direct integration method. This program can be regarded as the root-finding problem of a numerical function $F(\omega)$. A QNM can be found iteratively with a beginning tentative ω sufficiently close to it. The two methods will be introduced in detail in Sec. III.

III. METHOD

In our study, we employ the continued fractions technique to evaluate λ for angular parts and use both methods to determine ω. The comparison of the two methods is presented in Sec. IV C.

A. Continued fractions method

The well-known Teukolsky equation with any spin was solved by the continued fractions method on the background of Kerr BHs. In the seminal work by Leaver [49], both the QNM frequency and the separation constant are calculated using the continued fractions method.

Generally, the continued fractions method applies to most second order linear homogeneous differential equations with variable z defined within the unit circle $0 < |z| < 1$ [21]. The singularities of the equation should be removed outside the unit circle by redefining the coordinates for the convergence of the Frobenius series.[1] We develop a new code, which is slightly different from Leaver's work.

Let us start with the construction of the Frobenius series,

$$R(r) = \left(\frac{r - r_+}{r - r_-}\right)^A \left(\frac{r_\alpha - r}{r - r_-}\right)^B \sum_{i=0}^{N} a_i \left(\frac{r - r_+}{r - r_-}\frac{r_\alpha - r_-}{r_\alpha - r_+}\right)^i, \tag{11}$$

$$Y(\theta) = \left(\frac{\cos\theta - 1}{2}\right)^C \left(\frac{\cos\theta + 1}{2}\right)^D \sum_{i=0}^{K} b_i \left(\frac{\cos\theta + 1}{2}\right)^i, \tag{12}$$

where the two series are truncated to order N, K, respectively. The Frobenius series are imposed as the boundary behaviors from the boundary conditions (9) for $R(r)$ and (10) for $Y(\theta)$. All singular points appearing in equations are removed outside the unit circle through the definition of series. We will introduce the radial part as a template because both parts share the same code in the following discussion.

Substituting (11) into radial equation (5), in general, one can obtain an N-term recurrence relation

$$\sum_{j=0}^{\min(N-1,i)} \bar{\beta}_{j,i}^{(N)} a_{i-j} = 0, \quad \text{for } i > 0. \tag{13}$$

The algebraic relation between coefficients a_i allows one to reduce (13) to a three-term recurrence relation

$$\beta_{0,i}^{(3)} a_i + \beta_{1,i}^{(3)} a_{i-1} + \beta_{2,i}^{(3)} a_{i-2} = 0, \quad \text{for } i > 1,$$
$$\beta_{0,1}^{(3)} a_1 + \beta_{1,1}^{(3)} a_0 = 0, \tag{14}$$

step by step through an iterative program, where β_i is constituted by $\bar{\beta}_j$ as a function of system parameters. The resulting continued fractions equation is given by

---

[1]One can apply the continued fractions method beyond the convergence condition, as discussed in Appendix of [28].

$$\beta_{1,1}^{(3)} - \frac{\beta_{0,1}^{(3)}\beta_{2,2}^{(3)}}{\beta_{1,2}^{(3)} - \frac{\beta_{0,2}^{(3)}\beta_{2,3}^{(3)}}{\beta_{1,3}^{(3)} - \cdots}} = 0, \tag{15}$$

while we express a_1/a_0 from the two equations in (14) [49]. The equation above holds while ω is the QNM frequencies.

B. Direct integration method

The direct integration method has been introduced by Pani [50] and employed to coupled perturbation equations [51–53] or even the perturbations on the numerical solution of hairy BHs [54,55]. It is a powerful method competent for the decoupled perturbation equations of the analytic system in this paper. The main idea is to match two nontrivial solutions from opposite boundaries with corresponding boundary conditions (9) at an arbitrary midpoint r_m. The ingoing solution R_{in} integrating from the event horizon must be proportional to the outgoing solution R_{out} integrating from the acceleration horizon, while eigenvalue ω of the solutions is QNM frequency.

This method begins with constructing the series approximation at boundaries,

$$S_{\text{in}}(r) = (r - r_+)^A \sum_{i=0}^{N} c_i (r - r_+)^i, \quad \text{at } r_+, \tag{16}$$

$$S_{\text{out}}(r) = (r_\alpha - r)^B \sum_{i=0}^{N} d_i (r_\alpha - r)^i, \quad \text{at } r_\alpha. \tag{17}$$

These series are truncated to order N. Plugging (16) into the radial equation (5) one can solve the expression for each c_i in terms of c_0. c_0 is set to a nonvanishing constant (such as 1 in this paper) for approximating nontrivial solutions. This solved series can be used as an approximate boundary condition of ingoing solution R_{in} near the event horizon

$$R_{\text{in}}(r_+ + \epsilon) = S_{\text{in}}(r_+ + \epsilon), \tag{18}$$

with some small value ϵ. Then R_{in} is integrated from $r_+ + \epsilon$ to r_m. The procedure for solving R_{out} is similar. As a result, one can construct the determinant,

$$\text{Det} = \begin{vmatrix} R_{\text{in}}(r_m) & \partial_r R_{\text{in}}(r_m) \\ R_{\text{out}}(r_m) & \partial_r R_{\text{out}}(r_m) \end{vmatrix}. \tag{19}$$

The QNMs are obtained by imposing $\text{Det} = 0$.

IV. RESULTS

We investigate the QNM spectrum of rotating accelerating BHs. The mass M is fixed to 1 and hence all the physical quantities below are written as the simple dimensionless forms with M such as $M\omega = \omega$. We only present
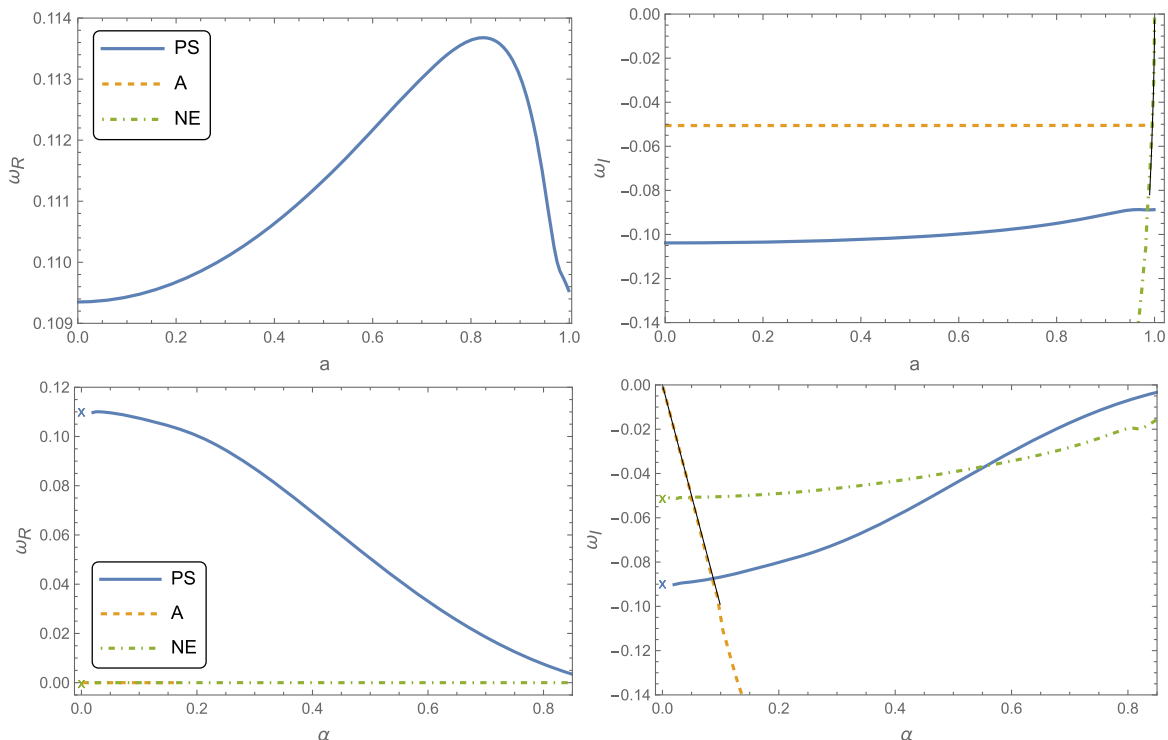
FIG. 1. Real (left) and imaginary (right) parts of $n = 0$ modes for both three families vs a (upper) with $m_0 = 0$, $\alpha = 0.05$ or vs α (bottom) with $m_0 = 0$, $a = 0.995$. The markers "x" denote the QNM value in the Kerr limit ($\alpha = 0$) determined by Leaver's work. The black lines are calculated by the formula (20) in bottom right panel or (21) in the upper right panel, which provide very good approximant to QNMs.

the mode with the separation constant λ with the largest real part (i.e., $l = m_0$ for the Schwarzschild case) in this paper.

A. Spectrum

We identify three families of scalar QNMs, including photon sphere (PS) modes, acceleration (A) modes, and near extreme (NE) modes, in the spectrum of the spinning C-metric under the scalar perturbation. The fundamental mode (also called the dominant mode) corresponds to the slowest damped mode in the QNM spectrum. However, the presence of three distinct families of modes necessitates a distinguishable labeling convention. Specifically, for given parameters (m_0, a, α), we refer to the $n = 0$ mode as the mode with the largest imaginary part for each of the three families and label the overtones for each of the three families as $n = 1, 2, \dots$. We also adopt a convention of utilizing subscripts in the abbreviation for each QNM family (e.g., PS_0 to denote the $n = 0$ photon sphere mode). The fundamental mode can be determined by comparing the $n = 0$ modes of each QNM family.

Figure 1 illustrates the behavior of the $n = 0$ modes for each family as a function of the parameter a or α. Both the real and imaginary parts of the PS_0 modes depicted by the blue line converge to zero with increasing α, but remain finite values while $a \to 1$. In the extreme BH limit ($a \to 1$), the near extreme modes become dominant in the QNM

spectrum and tend to be on the real axis with a vanishing imaginary part, as demonstrated by the green line in the upper right panel of Fig. 1. On the other hand, the bottom right panel of Fig. 1 demonstrates that the acceleration modes (the yellow line) become the fundamental modes in the limit $\alpha \to 0$, in which the acceleration horizon tends to radial infinity. This QNM spectrum shares similarities with those observed in prior works of the charged C-metric [28] and the RN-dS BH [30]. We introduce the three families of QNMs in the following.

1. Photon sphere modes ω_{PS}

The photon sphere is defined as the trapping region of BHs where null particles are forced to travel in circular unstable orbits. In the eikonal limit ($m \sim l \gg 1$), the decay timescale ω_I of the PS mode is directly related to the instability timescale of null geodesics near the photon sphere. The oscillation frequency ω_R of PS modes is associated with the orbital frequency of null geodesics [56,57].

2. Acceleration modes ω_A

Acceleration modes exclusively arise from the damped perturbations in the boosted spacetime. The imaginary part of acceleration modes exhibits a linear relationship with the surface gravity at the acceleration horizon of the Rindler space,
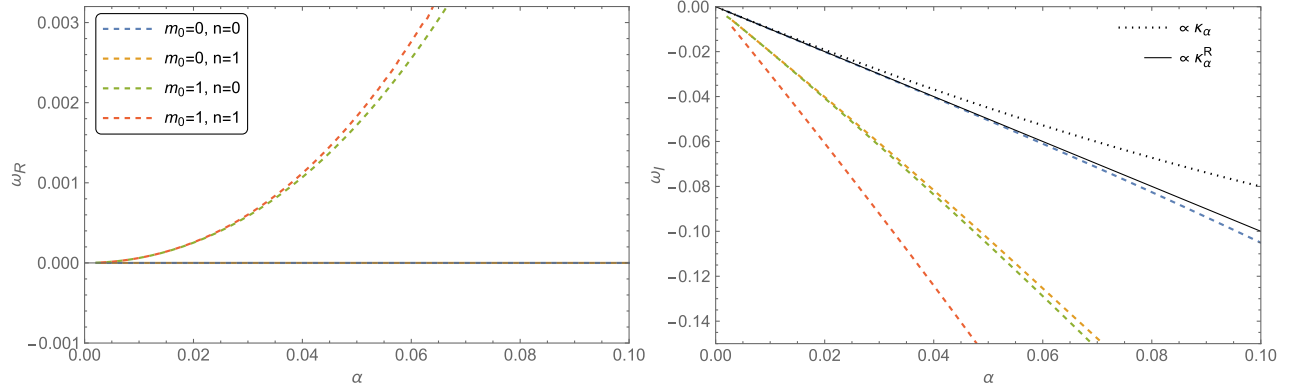
FIG. 2. Real (left) and imaginary (left) part of acceleration modes with different n, m_0 vs α on the background of rotating accelerating BHs where $a = 0.6$. The black solid line is depicted by formula (20) with $m_0 = n = 0$, and the black dotted lines are using the same formula while replacing κ_α^R by κ_α. The formula (20) characterized by κ_α^R can provide better approximant than that by κ_α.

$$\text{Im}(\omega_A) \simeq -\kappa_\alpha^R(m + n + 1)i, \qquad (20)$$

with only a weak dependence on the rotation parameter. It is intriguing that the acceleration modes in a BH spacetime exhibit a dependence on κ_α^R rather than the surface gravity κ_α for the accelerating BH, which was first reported in [28]. We depict the relationship (20) by the black line in the bottom right panel of Fig. 1, which is well consistent with the numerical results of acceleration modes. The intriguing dependence is also evident in the de Sitter modes for the RN-dS BH, which can be attributed to the role of the surface gravity at the cosmological horizon in governing the accelerated expansion of the RN-dS spacetime [30].

We show the acceleration modes with difference m_0 and n in Fig. 2. The black solid line represents the formula (20) and the black dotted line employs the same formula but replacing κ_α^R by κ_α. It is obvious that the linear dependence on κ_α^R provides the better approximant. By comparing Figs. 1 and 2, the acceleration modes are seen to emerge from the zero mode ($\omega = 0$), which is related to a constant solution for the radial equation (5) [31]. In the left part of Fig. 2, we have the acceleration modes with nonvanishing

real part, while the nonzero m_0 breaks the symmetry $\omega_R \rightarrow -\omega_R$. The effect of the BH on these modes may be encoded in the modified azimuth number m and its real part.

3. Near extreme modes ω_{NE}

The third family of QNMs appears in the limit where the location of the Cauchy horizon and event horizon tend to coincide. We also found an approximation while $a \rightarrow 1$,

$$\text{Im}(\omega_{\text{NE}}) \simeq -\kappa_-(n + 1)i, \qquad m_0 = 0, 1, \qquad (21)$$

$$\text{Im}(\omega_{\text{NE}}) \simeq -\kappa_-(n + 1/2)i, \qquad m_0 \geq 2. \qquad (22)$$

Such modes, branching with the familiar damped modes beyond a critical value of a, have been found in the spectrum of Kerr BHs and were called zero damping modes. The approximation given in (22) is accurately consistent with the analytic prediction presented in [38,39] with sufficient large a and small α. Remarkably, many similarities exist between the near extreme modes for the rotating Kerr BH and the charged version for the RN
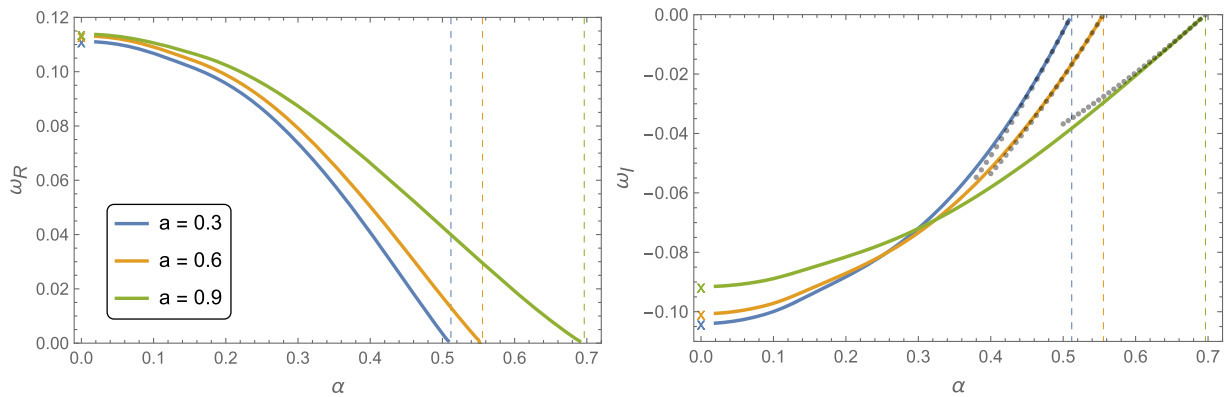
FIG. 3. Real (left) and imaginary (right) parts of PS_0 modes vs α with $m_0 = 0$. The BH rotation parameter a of different curves is shown in the frame. The dashed lines indicate the limit α_{ext}. The x markers denote QNM values in the Kerr limit ($\alpha = 0$) determined by Leaver' work and the gray dots are the analytic approximation $\text{Im}(\omega_{\text{PS}}) = -(n + 1/2)\kappa_+$ in the Nariai BH limit [37].
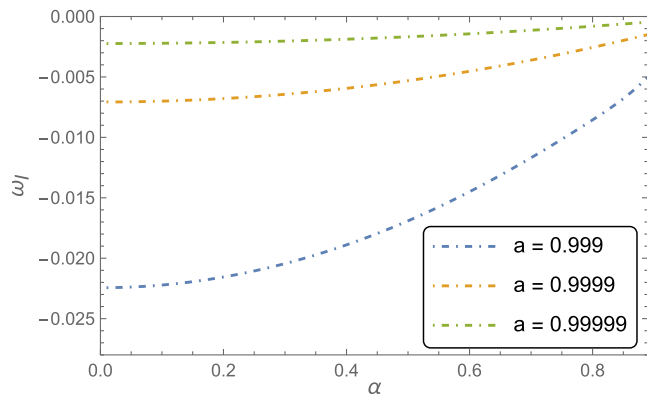
FIG. 4. Imaginary parts of $n = 0, m_0 = 0$ near extreme modes with different a vs α.

BH, although the physical interpretation of this correspondence remains unclear [30].

We present more details about the impact of acceleration α on the PS_0 modes in Fig. 3. The PS_0 modes with difference a become the zero mode characterized by vanishing real and imaginary parts in the limit $\alpha \to \alpha_{ext}$. The limit values α_{ext} for difference a are depicted by the dashed lines, respectively. When $\alpha \to \alpha_{ext}$, the rotating accelerating BH becomes the near Nariai-type extremal BH in which the event and acceleration horizon radii approach each other. Then the scalar perturbation equation produces a Pöshl-Teller potential and one can determine the QNMs with an analytic approach [37]. We depict the analytic approximant $\text{Im}(\omega_{PS}) = -(n + 1/2)\kappa_+$ with the gray dots in Fig. 3. The analytic approximant is in good agreement with our numerical results.

Similar trends are observed in Fig. 4, where we show the NE_0 modes with increasing α. However, due to the limitation of numerical calculation, we cannot provide conclusive evidence as to whether or not the near extreme mode also becomes zero mode when $\alpha \to \alpha_{ext}$.
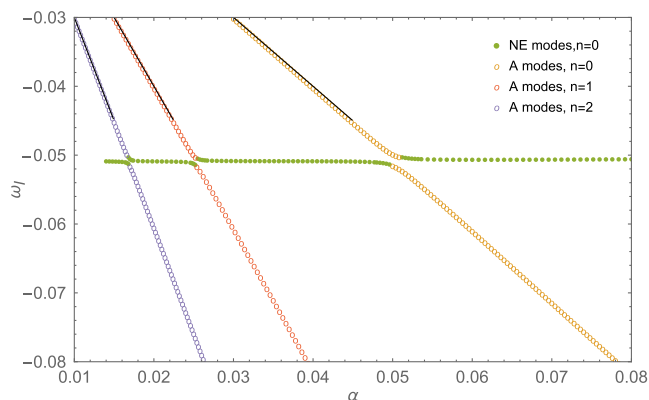
FIG. 5. The eigenvalue repulsion of A_i families and NE_0 modes with $m_0 = 0, a = 0.995$. There are frequency gaps in the neighborhood of two kinks of the two corresponding curves generating from the connection between A_i modes (for any $i = 0, 1, \dots$) and NE_0 modes. The black lines are depicted by formula (20).
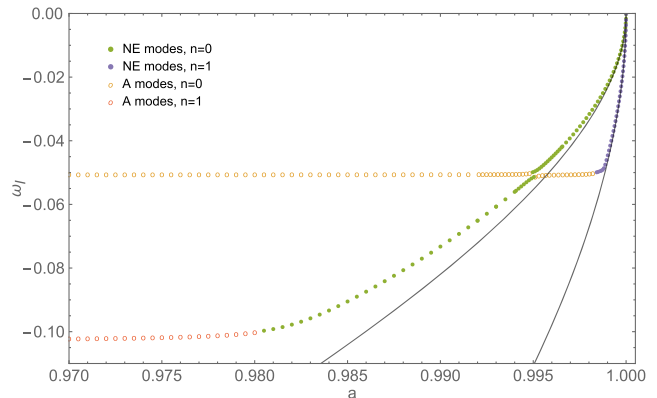
FIG. 6. The eigenvalue repulsion among A_0 modes, A_1 modes, NE_0 modes, and NE_1 modes with $m_0 = 0, \alpha = 0.2$ while varying a. The solid lines are evaluated by (21) with $n = 0$ and 1, respectively.

The eigenvalue repulsion phenomenon emerges while the A_0 line intersects with the NE_0 line in Fig. 1. We presented the magnified plots (Figs. 5 and 6 corresponding to the bottom right panel and the upper right panel of Fig. 1, respectively) for the further examination of this phenomenon.

In Fig. 5, each acceleration mode exhibits a rapid decrease with increasing α, while the NE_0 modes vary slightly. As a crossover of two lines occurs, both the A_0 line and the NE_0 line break into two pieces and connect with each other. Consequently, a gap emerges between the two kinks of the two new curves, diminishing the distinction between the different families. However, the black line calculated using (20) can still serve to distinguish between the two modes. Similar phenomenons are observed while the A_1 line and A_2 line intersect with the NE_0 line.

In Fig. 6, a similar eigenvalue repulsion is presented. This phenomenon arises when the acceleration modes encounter the increasing near extreme modes at the imaginary axis while a increases. The NE_0 line breaks into two pieces and the upper branch of this line connects smoothly to the A_0 family. Below, a continuous curve including four modes exists. With increasing a, the A_1 line connects to the bottom part of the NE_0 line, and then the right part of the A_0 line bridges the bottom part of the NE_0 line and the NE_1 line. There is also a gap between the kinks of the two continuous lines.

B. Strong cosmic censorship conjecture

We follow the derivation from the case of Kerr-dS BHs presented in [45]. One can convert the coordinates (t, r, θ, ϕ) into the outgoing coordinates (u, r, θ, ϕ') where the definition of new coordinates is given by

$$dt = du + \frac{r^2 + a^2}{Q} dr, \qquad d\phi = d\phi' + \frac{a}{Q} dr. \qquad (23)$$
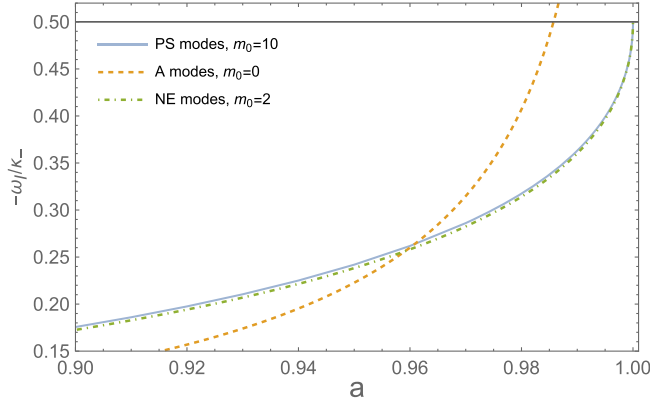
FIG. 7. $-\mathrm{Im}(\omega)/\kappa_-$ for each family of QNMs with $\alpha = 0.05$. The β is obtained by extracting the minimum value among three families.

Then the corresponding separable solution is imposed by

$$\varphi(u, r, \theta, \phi') = \Omega e^{-i\omega u} e^{im\phi'} R(r) \frac{Y(\theta)}{\sqrt{P}}. \qquad (24)$$

Now there are two independent solutions near the Cauchy horizon,

$$\varphi^{(1)} = \Omega e^{-i\omega u} e^{im\phi'} R^{(1)}(r) Y(\theta)/\sqrt{P}, \qquad (25)$$

$$\varphi^{(2)} = \Omega e^{-i\omega u} e^{im\phi'} (r - r_-)^{i[\omega - am/(r_-^2 + a^2)]/\kappa_-}$$
$$\times R^{(2)}(r) Y(\theta)/\sqrt{P}, \qquad (26)$$

with some nonzero functions $R^{(1)}(r)$ and $R^{(2)}(r)$. The regularity of QNMs is determined by the nonsmooth solution $\varphi^{(2)}$. The violation of SCC requires $\varphi^{(2)}$ to be locally square integrable, i.e., the condition that $(\partial_r \varphi^{(2)})^2$ is integrable gives

$$\beta > 1/2 \quad \text{where } \beta \equiv -\frac{\mathrm{Im}(\bar{\omega})}{\kappa_-}, \qquad (27)$$

where $\bar{\omega}$ denotes the fundamental modes in the spectrum. In other words, if a QNM ω with $-\mathrm{Im}(\omega)/\kappa_- < 1/2$ is discovered, one can determine that the SCC conjecture is respected under such perturbation for the given parameters (α, a). We depict $-\mathrm{Im}(\omega)/\kappa_-$ for each family of QNMs in Fig. 7 and demonstrate that the minimum value among the three families is always below $1/2$. These results can be expected from (22), where the imaginary part of near extreme modes with $n = 0$, $m_0 \geq 2$ are proportional to $-i\kappa_-/2$ while $a \to 1$. On the other hand, the charged version of near extreme modes with $n = l = 0$ is proportional to $-i\kappa_-$ in RN-dS BHs or the charged C-metric [28,30]. The different behaviors of modes in the extreme BH limit lead to different fates of SCC between charged and rotating BHs.

C. Comparison of methods

The Table I shows QNMs calculated by the continued fractions method and the direct integration method,

TABLE I.   The comparison between two methods with different parameters. We display only the $n = 0$ mode for each family. There are some modes not provided because they are higher overtones at such parameter values, which is difficult to be determined by numerical methods. As shown in this table, the two methods generally provide more consistent and accurate results for lower overtones. The first row with the separation constant $\lambda = -1.09236715$ regains the results given in [28], where the separation constant requires a transformation $\lambda' = -2\lambda + 1/3$.

Parameters	Families	Continued fractions method	Direct integration method
$\alpha = 0.03$	PS_0	$0.30327363 - 0.09736685i$	$0.30327413 - 0.09736639i$
$a = 0$	A_0	$-0.06189986i$	$-0.06189984i$
$m_0 = 1$	NE_0	$\cdots$	$\cdots$
$\alpha = 0.2$	PS_0	$0.09888222 - 0.08707878i$	$0.09888222 - 0.08707878i$
$a = 0.6$	A_0	$-0.21156725i$	$-0.21156725i$
$m_0 = 0$	NE_0	$\cdots$	$\cdots$
$\alpha = 0.1$	PS_0	$0.10742075 - 0.08685416i$	$0.10742077 - 0.08685417i$
$a = 0.995$	A_0	$-0.10804081i$	$-0.10804147i$
$m_0 = 0$	NE_0	$-0.05043962i$	$-0.05043962i$
$\alpha = 0.05$	PS_0	$\cdots$	$\cdots$
$a = 0.99998$	A_0	$-0.05055091i$	$-0.05033569i$
$m_0 = 0$	NE_0	$-0.00315480i$	$-0.00315558i$
$\alpha = 0.9$	PS_0	$0.00187795 - 0.00176789i$	$0.00187795 - 0.00176789i$
$a = 0.999$	A_0	$\cdots$	$\cdots$
$m_0 = 0$	NE_0	$-0.00453841i$	$-0.00453841i$
$\alpha = 0.15$	PS_0	$0.10113821 - 0.09480198i$	$0.10113821 - 0.09480198i$
$a = 0.1$	A_0	$-0.16337640i$	$-0.16337637i$
$m_0 = 0$	NE_0	$\cdots$	$\cdots$

TABLE II.   The comparison between QNMs and the approximants from (20)–(22) or the analytic formula $\mathrm{Im}(\omega_{PS}) = -(n + 1/2)\kappa_+$ presented in [37]. The approximants only show imaginary parts. Some modes were not provided due to the limitations of the corresponding numerical methods.

Parameters	Families	Continued fractions method	Direct integration method	Approximation
$\alpha = 0.1$	NE_0	$1.20792690 - 0.00034947i$	$\cdots$	$-0.00035052i$
$a = 0.999999$	NE_1	$1.20792630 - 0.00104781i$	$\cdots$	$-0.00105157i$
$m_0 = 2$	NE_2	$1.20792713 - 0.00174452i$	$\cdots$	$-0.00175262i$
$\alpha = 0.05$	NE_0	$-0.00022301i$	$-0.00022617i$	$-0.00022315i$
$a = 0.9999999$	NE_1	$-0.00044604i$	$-0.00036142i$	$-0.0004463i$
$m_0 = 0$	NE_2	$-0.00066907i$	$\cdots$	$-0.00066944i$
$\alpha = 0.002$	A_0	$\cdots$	$-0.00200002i$	$-0.002i$
$a = 0.5$	A_1	$\cdots$	$-0.00399363i$	$-0.004i$
$m_0 = 0$	A_2	$\cdots$	$-0.00599757i$	$-0.006i$
$\alpha = 0.508$	PS_0	$\cdots$	$0.00088583 - 0.0018015i$	$-0.00179944i$
$a = 0.3$	PS_1	$\cdots$	$0.00092112 - 0.0053762i$	$-0.00539831i$
$m_0 = 0$	PS_2	$\cdots$	$0.00054932 - 0.00908775i$	$-0.00899718i$

respectively. The two methods provide precisely consistent results. We also present QNMs with some extreme parameter choices (e.g., $a \to 1$ for the first two rows, $\alpha \to 0$ for the third row, and $\alpha \to \alpha_{\max}$ for the fourth row) in Table II. At such limit, only one method can give effective results, and its imaginary part matches the corresponding approximant. Another method becomes numerically unstable or provides unreliable discontinuous results. We show that the computable parameter spaces of the two methods are complementary.

V. DISCUSSION

This study focuses on the scalar ($s = 0$) QNM spectrum of rotating accelerating BHs calculated numerically by two methods (the continued fractions method and the direct integration method). Three families of QNMs are identified, namely photon sphere modes, acceleration modes, and near extreme modes. We examine the dependence of each family on various parameters, such as BH rotation and acceleration. We found that the acceleration modes demonstrate a linear dependence with the surface gravity κ_α^R at the acceleration horizon of Rindler space in the small BH limit ($\alpha \to 0$), while the near extreme modes are consistent with (21) in the extreme BH limit ($a \to 1$). The photon sphere modes become dominant and tend to zero mode while α approaches its extreme value α_{ext}. Our results are reliable because of the good agreement of the comparison between the two methods or the analytic approximations in previous works. We also discuss the eigenvalue repulsion phenomenon that occurs when the acceleration modes intersect with the near extreme modes at certain values of parameters. The distinction between different families of modes is diminished or even destroyed by the eigenvalue repulsion. The SCC conjecture is determined by β. We found no evidence of SCC violation.

The gravitational ($s = -2$) and electromagnetic ($s = -1$) perturbation of rotating accelerating BHs are still open problems. The precise dependence of acceleration modes on the surface gravity in the Rindler space suggests that these modes may exist beyond the spinning C-metric with axial symmetry. We deduce that, for rotating BHs or even compact objects without event horizon with arbitrary acceleration directions, the imaginary part of their acceleration modes should be approximately equal to the numerical results presented in this paper. When the BH has a sufficient small acceleration, such modes become the dominant or even the fundamental modes in the gravitational wave spectrum. Information about BHs, such as their spin and acceleration direction, may be encoded in the real part of their acceleration modes. Therefore, providing a ringdown template may enable us to search for moving and accelerating BHs in gravitational wave signals. This then offers another way alternative to the gravitational lensing [58] to distinguish slowly accelerating BHs.

[1] B. P. Abbott *et al.* (LIGO Scientific and Virgo Collaborations), Properties of the Binary Black Hole Merger GW150914, Phys. Rev. Lett. **116,** 241102 (2016).

[2] D. A. Brown, K. Vahi, M. Taufer, V. Welch, and E. Deelman, Reproducing GW150914: The first observation of gravitational waves from a binary black hole merger, Comput. Sci. Eng. **23,** 73 (2021).

[3] B. P. Abbott *et al.* (LIGO Scientific and Virgo Collaborations), Observation of Gravitational Waves from a Binary Black Hole Merger, Phys. Rev. Lett. **116,** 061102 (2016).

[4] K. Akiyama *et al.* (Event Horizon Telescope Collaboration), First M87 Event Horizon Telescope results. I. The shadow of the supermassive black hole, Astrophys. J. Lett. **875,** L1 (2019).

[5] P. T. Chrusciel, J. Lopes Costa, and M. Heusler, Stationary black holes: Uniqueness and beyond, Living Rev. Relativity **15,** 7 (2012).

[6] E. T. Newman, R. Couch, K. Chinnapared, A. Exton, A. Prakash, and R. Torrence, Metric of a rotating, charged mass, J. Math. Phys. (N.Y.) **6,** 918 (1965).

[7] J. F. Plebanski and M. Demianski, Rotating, charged, and uniformly accelerating mass in general relativity, Ann. Phys. (N.Y.) **98,** 98 (1976).

[8] J. B. Griffiths and J. Podolsky, A new look at the Plebanski-Demianski family of solutions, Int. J. Mod. Phys. D **15,** 335 (2006).

[9] G. J. Weir and R. P. Kerr, Diverging type-D metrics, Proc. R. Soc. A **355,** 31 (1977).

[10] W. Kinnersley, Type D vacuum metrics, J. Math. Phys. (N.Y.) **10,** 1195 (1969).

[11] J. B. Griffiths and J. Podolsky, Accelerating and rotating black holes, Classical Quantum Gravity **22,** 3467 (2005).

[12] H. Farhoosh and R. L. Zimmerman, Surfaces of infinite redshift around a uniformly accelerating and rotating particle, Phys. Rev. D **21,** 2064 (1980).

[13] J. Bicak and V. Pravda, Spinning C metric: Radiative spacetime with accelerating, rotating black holes, Phys. Rev. D **60,** 044004 (1999).

[14] K. Hong and E. Teo, A new form of the rotating C-metric, Classical Quantum Gravity **22,** 109 (2005).

[15] J. B. Griffiths and J. Podolsky, Global aspects of accelerating and rotating black hole space-times, Classical Quantum Gravity **23,** 555 (2006).

[16] D. Merritt, M. Milosavljevic, M. Favata, S. A. Hughes, and D. E. Holz, Consequences of gravitational radiation recoil, Astrophys. J. Lett. **607,** L9-L12 (2004).

[17] B. Bruegmann, J. A. Gonzalez, M. Hannam, S. Husa, and U. Sperhake, Exploring black hole superkicks, Phys. Rev. D **77,** 124047 (2008).

[18] D. Gerosa and C. J. Moore, Black Hole Kicks as New Gravitational Wave Observables, Phys. Rev. Lett. **117,** 011101 (2016).

[19] J. Calderón Bustillo, J. A. Clark, P. Laguna, and D. Shoemaker, Tracking Black Hole Kicks from Gravitational Wave Observations, Phys. Rev. Lett. **121,** 191102 (2018).

[20] U. Sperhake, E. Berti, V. Cardoso, F. Pretorius, and N. Yunes, Superkicks in ultrarelativistic encounters of spinning black holes, Phys. Rev. D **83,** 024037 (2011).

[21] R. A. Konoplya and A. Zhidenko, Quasinormal modes of black holes: From astrophysics to string theory, Rev. Mod. Phys. **83,** 793 (2011).

[22] K. D. Kokkotas and B. G. Schmidt, Quasinormal modes of stars and black holes, Living Rev. Relativity **2,** 2 (1999).

[23] E. Berti, V. Cardoso, and A. O. Starinets, Quasinormal modes of black holes and black branes, Classical Quantum Gravity **26,** 163001 (2009).

[24] Y. Zhao, B. Sun, Z. F. Mai, and Z. Cao, Quasi normal modes of black holes and detection in ringdown process, arXiv:2212.00747.

[25] J. D. Bekenstein, Black hole hair: 25—years after, arXiv:gr-qc/9605059.

[26] E. Berti, V. Cardoso, and C. M. Will, On gravitational-wave spectroscopy of massive black holes with the space interferometer LISA, Phys. Rev. D **73,** 064030 (2006).

[27] E. Berti, K. Yagi, H. Yang, and N. Yunes, Extreme gravity tests with gravitational waves from compact binary coalescences: (II) Ringdown, Gen. Relativ. Gravit. **50,** 49 (2018).

[28] K. Destounis, R. D. B. Fontana, and F. C. Mena, Accelerating black holes: Quasinormal modes and late-time tails, Phys. Rev. D **102,** 044005 (2020).

[29] K. Destounis, G. Mascher, and K. D. Kokkotas, Dynamical behavior of the C-metric: Charged scalar fields, quasinormal modes, and superradiance, Phys. Rev. D **105,** 124058 (2022).

[30] V. Cardoso, J. L. Costa, K. Destounis, P. Hintz, and A. Jansen, Quasinormal Modes and Strong Cosmic Censorship, Phys. Rev. Lett. **120,** 031103 (2018).

[31] V. Cardoso, J. L. Costa, K. Destounis, P. Hintz, and A. Jansen, Strong cosmic censorship in charged black-hole spacetimes: Still subtle, Phys. Rev. D **98,** 104007 (2018).

[32] T. W. Baumgarte and C. Gundlach, Critical Collapse of Rotating Radiation Fluids, Phys. Rev. Lett. **116,** 221103 (2016).

[33] C. Gundlach and T. W. Baumgarte, Critical gravitational collapse with angular momentum, Phys. Rev. D **94,** 084012 (2016).

[34] C. Gundlach and T. W. Baumgarte, Critical gravitational collapse with angular momentum II: Soft equations of state, Phys. Rev. D **97,** 064006 (2018).

[35] E. Berti, A. Sesana, E. Barausse, V. Cardoso, and K. Belczynski, Spectroscopy of Kerr Black Holes with Earth- and Space-Based Interferometers, Phys. Rev. Lett. **117,** 101102 (2016).

[36] B. P. Abbott *et al.* (LIGO Scientific and Virgo Collaborations), Tests of General Relativity with GW150914, Phys. Rev. Lett. **116,** 221101 (2016); Phys. Rev. Lett. **121,** 129902(E) (2018).

[37] B. Gwak, Quasinormal modes in near-extremal spinning C-metric, Eur. Phys. J. Plus **138,** 582 (2023).

[38] H. Yang, F. Zhang, A. Zimmerman, D. A. Nichols, E. Berti, and Y. Chen, Branching of quasinormal modes for nearly extremal Kerr black holes, Phys. Rev. D **87,** 041502 (2013).

[39] H. Yang, A. Zimmerman, A. Zenginoğlu, F. Zhang, E. Berti, and Y. Chen, Quasinormal modes of nearly extremal Kerr spacetimes: Spectrum bifurcation and power-law ringdown, Phys. Rev. D **88,** 044047 (2013).

[40] O. J. C. Dias, M. Godazgar, J. E. Santos, G. Carullo, W. Del Pozzo, and D. Laghi, Eigenvalue repulsions in the quasinormal spectra of the Kerr-Newman black hole, Phys. Rev. D **105**, 084044 (2022).

[41] O. J. C. Dias, M. Godazgar, and J. E. Santos, Eigenvalue repulsions and quasinormal mode spectra of Kerr-Newman: An extended study, J. High Energy Phys. 07 (2022) 076.

[42] A. Davey, O. J. C. Dias, P. Rodgers, and J. E. Santos, Strong Cosmic Censorship and eigenvalue repulsions for rotating de Sitter black holes in higher-dimensions, J. High Energy Phys. 07 (2022) 086.

[43] M. Dafermos, The interior of charged black holes and the problem of uniqueness in general relativity, Commun. Pure Appl. Math. **58**, 0445 (2005).

[44] J. Luk and S. J. Oh, Strong cosmic censorship in spherical symmetry for two-ended asymptotically flat initial data I. The interior of the black hole region, arXiv:1702.05715.

[45] O. J. C. Dias, F. C. Eperon, H. S. Reall, and J. E. Santos, Strong cosmic censorship in de Sitter space, Phys. Rev. D **97**, 104060 (2018).

[46] K. Destounis, R. D. B. Fontana, and F. C. Mena, Stability of the Cauchy horizon in accelerating black-hole spacetimes, Phys. Rev. D **102**, 104037 (2020).

[47] M. Zhang and J. Jiang, Strong cosmic censorship in accelerating spacetime, Sci. China Phys. Mech. Astron. **66**, 280412 (2023).

[48] D. Bini, C. Cherubini, and A. Geralico, Massless field perturbations of the spinning C metric, J. Math. Phys. (N.Y.) **49**, 062502 (2008).

[49] E. W. Leaver, An analytic representation for the quasi normal modes of Kerr black holes, Proc. R. Soc. A **402**, 285 (1985).

[50] P. Pani, Advanced methods in black-hole perturbation theory, Int. J. Mod. Phys. A **28**, 1340018 (2013).

[51] J. L. Blázquez-Salcedo, C. F. B. Macedo, V. Cardoso, V. Ferrari, L. Gualtieri, F. S. Khoo, J. Kunz, and P. Pani, Perturbed black holes in Einstein-dilaton-Gauss-Bonnet gravity: Stability, ringdown, and gravitational-wave emission, Phys. Rev. D **94**, 104024 (2016).

[52] L. Pierini and L. Gualtieri, Quasi-normal modes of rotating black holes in Einstein-dilaton Gauss-Bonnet gravity: The first order in rotation, Phys. Rev. D **103**, 124017 (2021).

[53] L. Pierini and L. Gualtieri, Quasinormal modes of rotating black holes in Einstein-dilaton Gauss-Bonnet gravity: The second order in rotation, Phys. Rev. D **106**, 104009 (2022).

[54] J. L. Blázquez-Salcedo, F. S. Khoo, and J. Kunz, Quasinormal modes of Einstein-Gauss-Bonnet-dilaton black holes, Phys. Rev. D **96**, 064008 (2017).

[55] J. L. Blázquez-Salcedo, D. D. Doneva, J. Kunz, and S. S. Yazadjiev, Radial perturbations of the scalarized Einstein-Gauss-Bonnet black holes, Phys. Rev. D **98**, 084011 (2018).

[56] V. Ferrari and B. Mashhoon, New approach to the quasinormal modes of a black hole, Phys. Rev. D **30**, 295 (1984).

[57] V. Cardoso, A. S. Miranda, E. Berti, H. Witek, and V. T. Zanchin, Geodesic stability, Lyapunov exponents and quasinormal modes, Phys. Rev. D **79**, 064016 (2009).

[58] A. Ashoorioon, M. B. Jahani Poshteh, and R. B. Mann, Distinguishing a Slowly Accelerating Black Hole by Differential Time Delays of Images, Phys. Rev. Lett. **129**, 031102 (2022).

Correction: The "corresponding author" identifier was removed from the byline footnote for the second author during the production cycle and has been restored.